ACOUSTICAL ANALYSIS OF A HUNGARIAN FOLK FLUTE

Péter Rucz[1], Noémie Kégl-Tourneix[2,3]

[1] *Dept. of Networked Systems and Services, Budapest University of Technology and Economics, Hungary*
[2] *Université de Bordeaux, CNRS, Bordeaux INP, LaBRI, UMR 5800, Talence, France*
[3] *Laboratoire de Phonétique et Phonologie, UMR 7018, CNRS, Université Sorbonne Nouvelle, Paris, France*

This paper is a revised version of the authors' submitted manuscript that was peer-reviewed by at least two anonymous reviewers.

Abstract

Studies on the sound generation by air reed instruments continue to reveal new details of their sound production mechanism. While a substantial body of knowledge is available on classical instruments, relatively few studies have focused on folk instruments. Hungarian folk flutes exhibit remarkable design diversity and can be grouped into regional types, each associated with distinct performance practices.
This study presents an acoustical analysis of a Hungarian folk flute, specifically a Transylvanian shepherd type. The investigation compares one-dimensional transmission matrix models and three-dimensional finite element simulations of the resonance properties of the air column with sound recordings obtained under laboratory conditions. In addition to documenting the acoustical features of the flute, the study reveals interesting resonance properties, including pitch sharpening by cross-fingerings, and an increase of apparent wavelength by the tone hole lattice.

Keywords: *air reed instruments, finite elements, folk flutes, sound analysis, transmission matrix model*

1. Introduction

Folk flutes were played throughout all the regions where the Hungarian language is spoken, with the instruments traditionally made by local craftsmen. Therefore, a large amount of diversity can be seen in the design of these flutes. As folk instruments and their music are an important part of our cultural heritage, the knowledge of traditional instrument making should be preserved. However, almost all of the master craftsmen have passed away. As a result, today's flute makers must rediscover much of the practical knowledge through experimentation and intuition. This paper presents a study of a specific flute with the aim of understanding and documenting its acoustical features, while also providing insights that may be useful for instrument makers.

Corresponding author: *rucz@hit.bme.hu.*

Table 1: Dimensions of the folk flute in mm units (uncertainty ±0.05 mm). Tone hole distances from lower lip.

Main bore		
Total length	368.20	
Length of foot	18.30	
Inner ⌀ (mouth, open end)	14.70	12.65
Wall thickness	3.25	2.40
Mouth window and windway		
Windway width and height	8.3	1.8
Mouth width and height	6.40	6.40
Length of ears	2.50	
Height of upper lip	24.10	
Tone holes	Distance	⌀
Hole 1	168.75	6.80
Hole 2	198.80	7.90
Hole 3	224.00	7.90
Hole 4	257.80	6.85
Hole 5	276.70	8.85
Hole 6	309.10	6.85

The lowest note of the studied flute is $A_4 \approx 440$ Hz. With six finger holes and overblowing, its musical range spans two and a half octaves, from A_4 to D_7, following a diatonic scale. The ash wood body has a total length of 386.5 mm, and the bore is slightly tapered towards the open end. Dimensions are listed in Table 1 and a photo is shown in Fig. 1. The mouth window is almost perfectly square, which is not usual for classical instruments, where the width of the window is commonly 2–4 times its height. The labium is on the side opposite the finger holes and faces downward when the instrument is played. With respect to the air-jet excitation, the short windway and the window geometry are the two main features that distinguish this fipple flute from classical recorders.

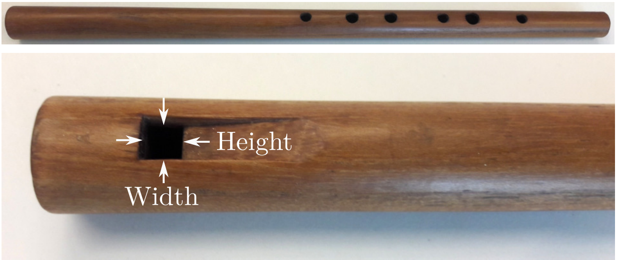

Figure 1: Photos of the Transylvanian shepherd flute. Top: full body. Bottom: zoom on the labium and foot.

2. Methodology

2.1. Transmission matrix model

Using a one-dimensional framework valid under the cutoff frequency of the resonator ($f_\mathrm{c} \approx 13.5\,\mathrm{kHz}$), a transmission matrix model (TMM) of the flute was constructed. This model consists of conical bore elements with wall losses computed using the theory of Zwikker & Kosten [1], tone hole models of Lefebvre & Scavone [2], and radiation impedances at the open end and the mouth window. By means of this model, the input admittance function $Y_\mathrm{in}(f)$ of the recorder is evaluated in the frequency domain, and the resonance frequencies are found at the maxima of Y_in.

2.2. Three-dimensional model

Three-dimensional finite element (FE) models of the flute with different fingerings were created using the parametric mesh generation tool Gmsh [3]. The air column enclosed in the flute body as well as a cylindrical portion of the surrounding air are meshed by tetrahedral elements, with the characteristic element size varying between 0.8 mm (near tone holes and the window) and 1.0 mm in the interior, and increases to 3.0 mm in the exterior field.

Astley – Leis infinite elements [4] are added to the cylindrical boundary around the flute to emulate free field conditions. Exploiting a symmetry plane aligned with the longitudinal section, the total number of acoustic pressure degrees of freedom in the discretized system was around 100 k, varying slightly with the open or closed states of the tone holes. To account for the fingertips partially extending into the tone holes, the chimney height of closed holes is uniformly taken as 1.5 mm rather than the actual wall thickness used for open holes. Wall losses due to friction and heat exchange were taken into account following the approach proposed by Berggren *et al.* [5]. Unfortunately, the input admittance cannot be attained directly from the FE model, therefore, an other approach was chosen. A monopole source, located in the axis of the flute at a distance of 2 m excited the acoustic resonances of the air column, leading to a scattering problem formulated assuming acoustically rigid walls. A transfer function from the source to a virtual receiver point located in the interior of the flute, opposing the mouth window was evaluated. Resonance frequencies are found at the local maxima of this transfer function.

The FE simulations were also performed in the frequency domain in the range $200 \leq f \leq 5000\,\mathrm{Hz}$, with a first frequency step of 20 Hz, and then refining by 1 Hz steps near the first five peaks. The 3D FE simulations took approximately 80 minutes altogether for one fingering on an average desktop PC. In both 1D and 3D models, the medium is air at $T = 27\,°\mathrm{C}$ temperature, approximating playing conditions. A total of 13 fingerings were studied, 10 of which are used in actual playing. All simulations presented in the paper were implemented by self-developed software codes.

2.3. Sound recordings and analysis

Sounds of steady notes played on the flute by an expert flutist were recorded in the semi-anechoic chamber of TU Budapest. Each note in the musical range was recorded three times to facilitate subsequent transient analyses as well as the evaluation of the statistics of the steady signals. The notes were played naturally, without tremolo or vibrato, and no further instructions were given to the performer. A few musical examples were recorded as well, with the player performing in his preferred style. Two B&K 4188 ½" calibrated condenser microphones were used for the recordings, one in the near field (distance 0.3 m) and the other in the far field (distance 2 m). The signals were digitized by a National Instruments NI-9234 24-bit module, at a sampling frequency of $f_\mathrm{s} = 51.2\,\mathrm{kHz}$.

The recordings were segmented into attack, steady state, and decay sections. The steady state signals were evaluated first, by precise fundamental frequency detection and resampling. Equivalent loudness and spectral centroid were calculated from the spectra. By frequency detection on consecutive sample blocks, small variations of the sounding frequencies could be evaluated for assessing the intonation profile.

3. Window impedance

The first comparison with all tone holes closed revealed a significant difference between the resonance frequencies estimated by the 1D and 3D models. It was suspected that the discrepancy stems from the radiation impedance model of the mouth window, as the window geometry of the folk flute differs remarkably from those of classical recorders. Therefore, the window impedance was simulated by 3D FEM as well, in the arrangement depicted in Fig. 2. A cylindrical body was assumed, neglecting the slight tapering of the real flute. The tube is excited by a plane wave prescribed as a Dirichlet boundary condition.

The mouth window impedance Z_m, reflection coefficient R_m, and end correction ΔL_m are related by

$$\frac{\hat{p}^+}{\hat{p}^-} = R_\mathrm{m} = -\left|R_\mathrm{m}\right| \mathrm{e}^{-2\mathrm{j}k\Delta L_\mathrm{m}} = \frac{Z_\mathrm{m} - Z_0}{Z_\mathrm{m} + Z_0}, \quad (1)$$

where $\hat{p}^+$ and $\hat{p}^-$ are complex magnitudes associated with the plane waves inside the resonator propagating away and toward the mouth, respectively. Z_0 is the plane wave impedance, and k is the wave number. The coefficients $\hat{p}^+$ and $\hat{p}^-$ were evaluated by the plane

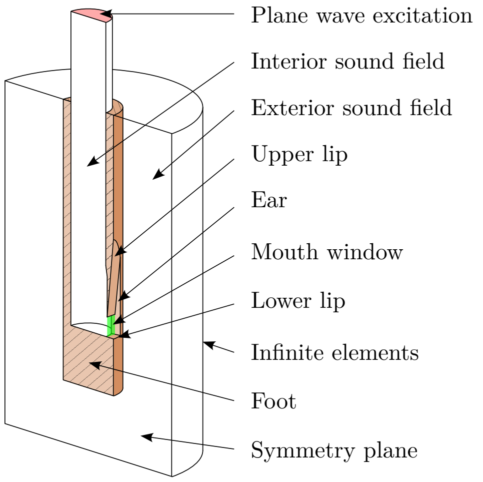

Figure 2: Arrangement of finite element simulations of the window impedance.

wave decomposition of the interior sound field.
Fig. 3 compares the end corrections ΔL_{m} attained from the FE simulations to the window models of Verge et al. [6] and Ernoult & Fabre [7]. The former model is theoretical, while the latter includes data fit formulas to measurements and simulations on simplified geometries. While previous investigations on classical instruments gave a much better agreement of the models [8], in case of the window geometry studied here, the discrepancies are significant. Interestingly, the model of Ernoult & Fabre gives greater, while the Verge model yields lower end correction values than those attained by the 3D simulations. The deviations of the end corrections are the greatest at low frequencies, which are the most important for predicting the first few resonance frequencies. The 13 mm difference in ΔL_{m} between the Ernoult model and FE is 3.5 % of the total length, which deviation is too high for comparing the resulting intonations. To eliminate the discrepancy of the mouth window models, the FE mouth impedance was used with the 1D TMM as well, referred to as hybrid model hereafter.

4. Analysis results

4.1. Loudness evaluation

The evaluation of the average steady state levels measured by the near field microphone is shown in Fig. 4. A clear increasing trend is observed toward higher pitches where notes are produced by overblowing, with the notes B_5, $\mathrm{C\#}_6$, D_6 representing an exception forming a dip in the measured levels. The differences of the levels of the highest and lowest pitches is as high as 31 dBSPL. The standard deviation of the levels was found as ≤ 1.1 dB for all notes. The diatonic scale can be played using the 1$^{\mathrm{st}}$ register in the first octave, the 2$^{\mathrm{nd}}$ register in the second octave, and the 3$^{\mathrm{rd}}$ register for the next three notes. The highest pitch (D_7, ≈ 2350 Hz), is sounded by exciting the 4$^{\mathrm{th}}$ longitudinal resonance of the air column.

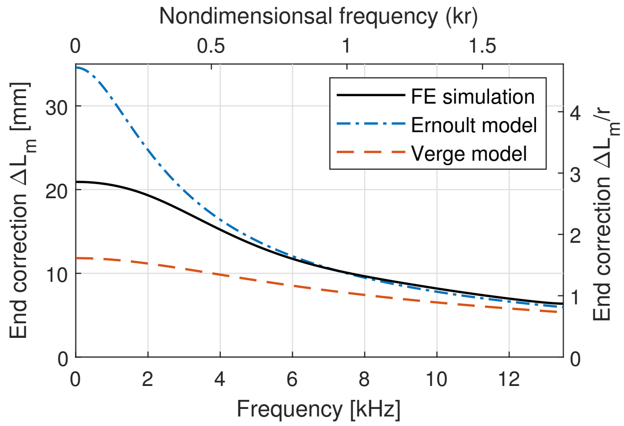

Figure 3: Comparison of FE mouth end corrections to two models from the literature.

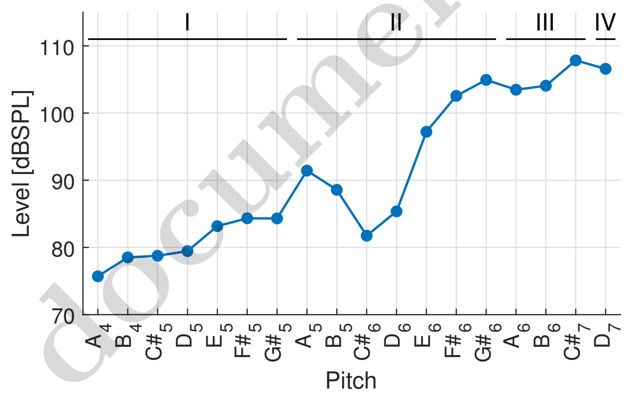

Figure 4: Average steady state levels measured by the near field microphone. Roman numbers: register index.

4.2. Spectra and admittance

It is interesting to compare the steady state spectra of the measured sounds with the input admittance functions computed by the 1D TMM. Fig. 5 displays these functions for the A_4, A_5, and A_6 notes. To facilitate the comparison, the spectra are displayed over a normalized frequency scale, where the unit is the fundamental frequency of the A_4 note. In case of A_4 (top diagram), a regular spectrum and admittance curve are observed as a result of all tone holes being closed. Naturally, the main components of the sound spectrum are the harmonic partials, found at integer normalized frequencies. The fundamental is the strongest component, and the third partial (pure fifth) is the second one with a relative level of -9 dB. Admittance peaks are also regular, but show a slight stretching compared to the harmonic partials, as a result of the end corrections decreasing with the frequency (see also Fig. 3). At higher frequencies, broader peaks of the sound spectrum coincide in frequency with admittance maxima. This result is explained by the resonator amplifying the broadband noise produced by the air jet and its interaction with the upper lip.
The middle diagram of Fig. 5 shows the first note of the 2$^{\mathrm{nd}}$ register, A_5. Compared to A_4, the fundamental

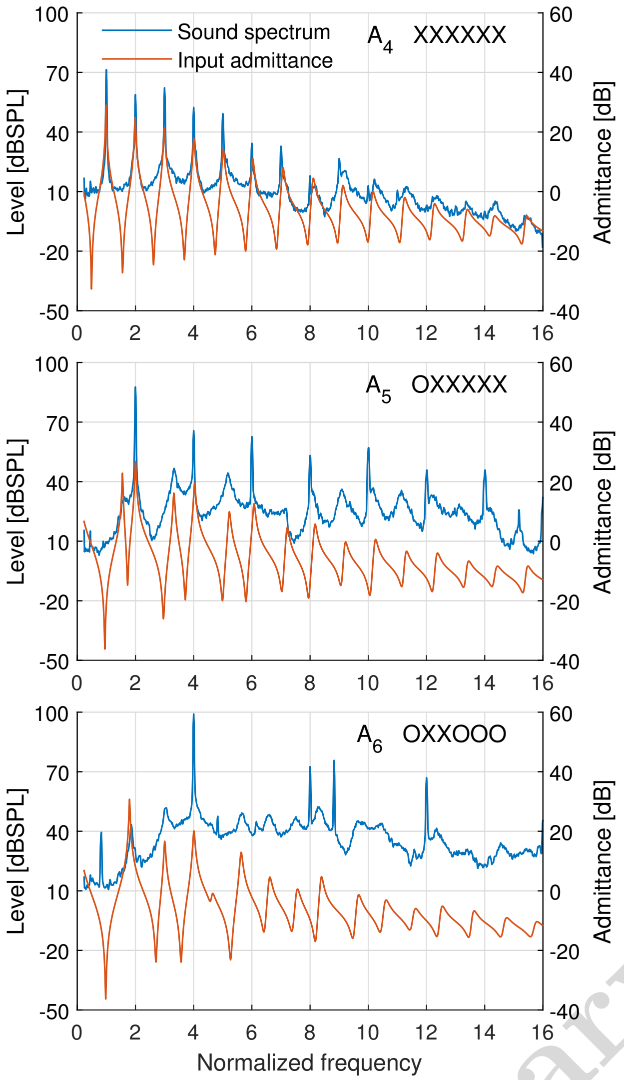

Figure 5: Steady state sound spectra and input admittance for notes A_4 (top), A_5 (middle), and A_6 (bottom).

is the strongest component here as well, but in this case the second partial (octave) comes next, with a relative level of only -22 dB. One can observe broad spectral peaks between the harmonic partials, for example at normalized frequencies of 3.33 and 5.17. This behavior is the combined result of the cross-fingering and overblowing. Due to the higher jet velocity the levels of the broad spectral peaks are also elevated compared to the A_4 note.

A similar effect is found in case of A_6, shown as the bottom diagram of Fig. 5. While the fundamental became even stronger, the relative level of the octave decreased to -26 dB. Interestingly, a sharp peak, 3 dB stronger than the octave, appears at the non-harmonic normalized frequency of 8.83. Similar peaks at slightly different frequencies were found in repeated recordings of this particular note. The origin of this non-harmonic component remains unknown.

A very good correspondence between the spectral baseline and the input admittance was found in all cases.

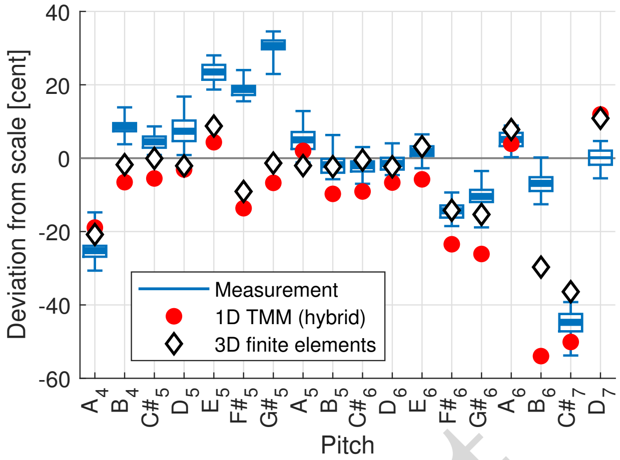

Figure 6: Comparison of intonation profiles from played notes and acoustical models. Box plot: thick horizontal lines are the mean values, the boxes represent the quartile values, and the whiskers denote the extrema.

Therefore, in the following, the resonance frequencies predicted by the acoustical models are compared in greater detail with the sounding frequencies.

4.3. Intonation profile

The intonation profile of the instrument represents the deviations of the sounding (or resonance) frequencies from those of the musical scale. Nagy *et al.* [9] compared a one-dimensional acoustical model to resonance measurements on a tenor recorder, while Bastien *et al.* [10] used input impedance measurements, an artificial player, and simulations by a jet-drive model for assessing the intonation profile of an alto recorder. Here, the resonance frequencies from the acoustical models are compared with the sounding frequencies evaluated from sound recordings. The equally tempered scale fitting best to the measured frequencies has $A_4^{\text{meas}} = 443.9$ Hz, while for the models $A_4^{\text{model}} = 440.0$ Hz is taken. This deviation of 15.3 cent stems from the lack of a jet-drive mechanism in the purely acoustical model [10], and slight differences of assumed and real material properties of air.

The intonation profiles from the measurements and the acoustical models are depicted in Fig. 6. Overall, a very good agreement of models and measurements is observed. The trends are captured well by both 1D TMM and 3D FEM. In particular, the under-tuning of the A_4 and $C\#_7$ notes are reproduced accurately. The mean and maximum absolute deviations from the measurements are 13 and 47 cent for the 1D TMM, and 9 and 32 cent in case of the 3D FEM, respectively. The best fits are found for the notes in the 2nd register, where the maximum deviations from the measurements are 16 and 7 cents for TMM and FEM, respectively. There are only four notes, where the difference between the models and measurement is greater than 20 cent: E_5, $F\#_5$, $G\#_5$ and B_6. For all these notes, the sounding frequency is higher than that predicted by the models.

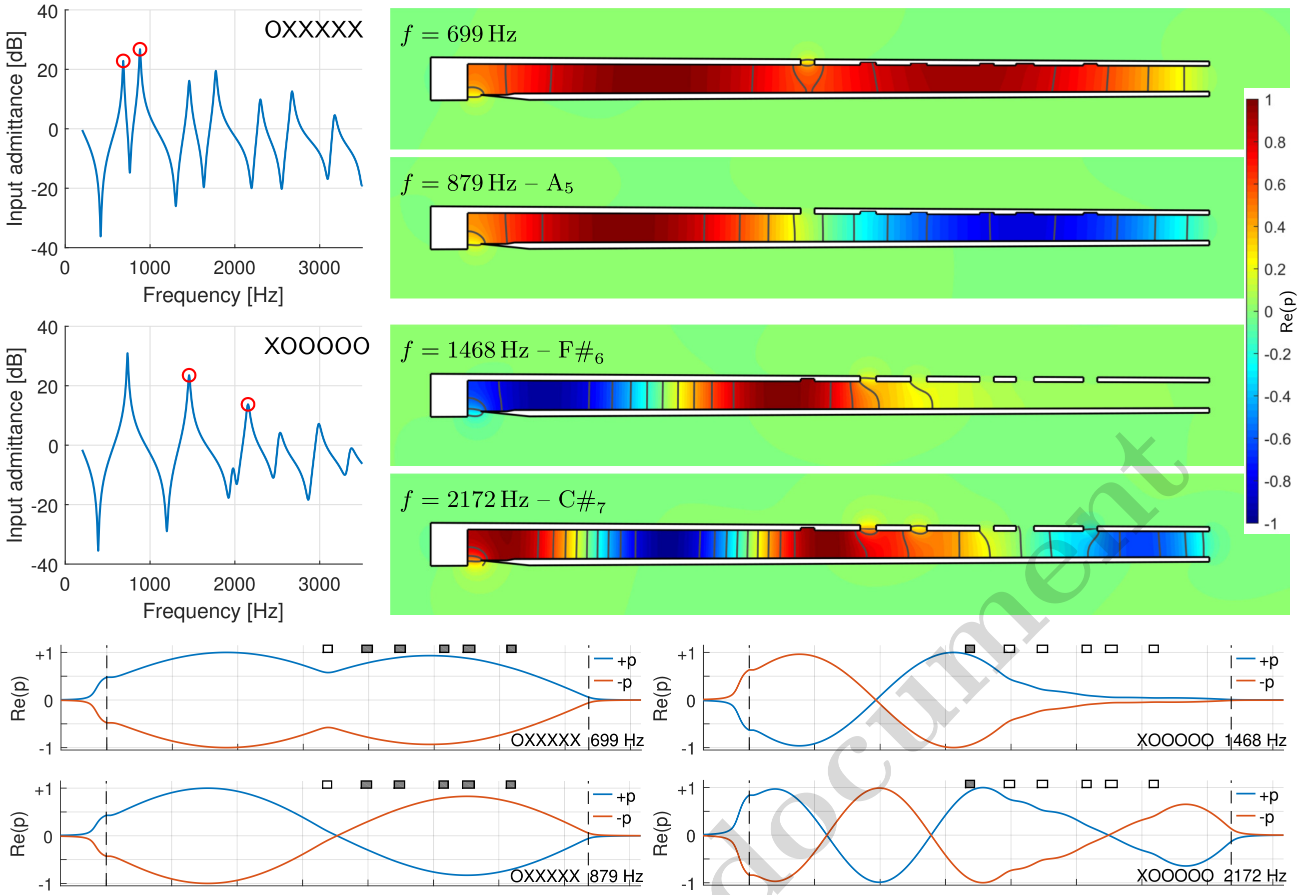

Figure 7: Acoustical resonances of the air column at characteristic admittance peaks. Bottom: sound pressure along the centerline of the bore with the dashed vertical lines indicating the position of the mouth and the open end. The colors and the bottom curves show the normalized real part of the scattered acoustic pressure field.

The average absolute deviation between the TMM and FEM is 7 cent across all notes, and the single note where the difference of the two models is greater than 20 cent is the B_6 note. The latter note is played with the XXOOOO fingering by exciting the third resonance. Both the TMM and FEM show that the corresponding resonance peak is the lower-frequency component of peak doublet. Such double peaks typically occur as a result of resonance splitting.

4.4. Examination of sound fields at resonance

While pressure waveforms along the bore axis can also be visualized using TMM results, the FEM model offers the distinct advantage of enabling straightforward visualization of the pressure field. Such visualizations help provide a better understanding of the resonances of the air column. Furthermore, the 3D model can also reveal the presence of non-planar wave components within the bore.

Fig. 7 shows two examples of interesting resonance phenomena observed in this study. The top diagram depicts the input admittance curve for the fingering of the A_5 note. Interestingly, near 800 Hz the admittance peak splits into two, producing two maxima with similar magnitudes. As visible, the first and second peaks respectively produce in-phase and anti-phase oscillations in the bore sections upstream and downstream of the open tone hole. This effect is known as the avoided crossing of two resonance frequencies, and it was examined by Adachi [11] on an alto recorder. While in the latter study the cross-fingering resulted in pitch sharpening in the 3$^{\text{rd}}$ register (concerning conventional fingerings only), here this effect is already exploited for producing the first note of the 2$^{\text{nd}}$ register. An interesting difference visible in the sound fields is that despite the open tone hole, the magnitude of the pressure wave remains high in the bore at the position of the tone hole in case of the in-phase oscillation. In the anti-phase case, the magnitude is near zero at the open tone hole. It is also noted that it is hard to achieve a steady sound exciting the lower-frequency peak of the doublet (near 700 Hz) by the air jet during playing: the sounding frequency jumps to that of A_5 (near 880 Hz) very easily as a result of a small increase of the blowing pressure.

The other case, illustrated in the bottom diagram of Fig. 7 is the inverted fingering, used for producing notes F$\#_5$, F$\#_6$, and C$\#_7$. The standing pressure waves corresponding to the two latter notes are shown. While in case of F$\#_6$, the open tone holes result in a vanishing magnitude towards the open end of the flute, for C$\#_7$ the standing wave remains considerably strong despite the open tone holes. Due to the effect of the open tone holes, the interior field oscillates in-phase in the bore section between holes 1 to 5, making the apparent wavelength in this portion of the bore longer. This effect is clearly visible in the bottom graphs of the figure, where the sound pressure along the centerline of the bore is depicted. While minor non-planar features of the sound field are observed in all cases near the labium and the open tone holes, they are more pronounced for the C$\#_7$ note due to the higher fundamental frequency. Clear non-planar effects are visible near the first two and the last open finger holes, as highlighted by the gray contours overlaid on the color plot.

5. Conclusions

This study examined a Hungarian folk flute using acoustical models and analysis of sound recordings. Two modeling approaches, a one-dimensional TMM and a three-dimensional FEM, were considered, and their predictions were compared with measured steady-state spectral features. The window impedance was found to be the main source of the differences between the 1D and 3D models. While analytical models are typically tailored to classical instruments, the height-to-width ratio of the mouth window of the examined folk flute differs significantly from that of classical recorders which most likely contributes to the observed discrepancies. These differences were resolved by a hybrid model that incorporates the mouth impedance derived from 3D FE simulations.

The comparison of steady state spectra and input admittance curves showed close agreement between models and measurements. Evaluation of the intonation profile confirmed that both models predict the sounding frequencies of the flute with excellent accuracy. Exploiting the FE model, the pressure waves at resonances of the air column could be directly visualized, revealing interesting effects associated with resonance splitting and local non-planar features of the sound field.

The hybrid model enables rapid computation of input admittance functions and resonance frequencies for a variety of fingerings. Such results may provide useful guidance for folk flute makers in refining their designs.

6. Acknowledgments

The authors gratefully thank Dániel Bolya (musician, music teacher, and flute maker – BolyaFlute) for providing the flute examined in this paper and participating in sound recordings. This work has been supported by the Hungarian National Research, Development and Innovation Office under contract No. Advanced–153066. N K-T acknowledges the Erasmus+ program for supporting her visiting semester in Hungary, and the Budapest University of Technology and Economics for making this project possible during her stay.

References

[1] C. Zwikker and C. W. Kosten, *Sound Absorbing Materials*. Elsevier, 1949.

[2] A. Lefebvre and G. P. Scavone, “Characterization of woodwind instrument toneholes with the finite element method,” *Journal of the Acoustical Society of America*, vol. 131, no. 4, pp. 3153–3163, 2012. DOI: 10.1121/1.3685481.

[3] C. Geuzaine and J.-F. Remacle, “Gmsh: A three-dimensional finite element mesh generator with built-in pre- and post-processing facilities,” *International Journal for Numerical Methods in Engineering*, vol. 79, no. 11, pp. 1309–1331, 2009. DOI: 10.1002/nme.2579.

[4] R. J. Astley, G. J. Macaulay, J.-P. Coyette, and L. Cremers, “Three-dimensional wave-envelope elements of variable order for acoustic radiation and scattering: Part I. Formulation in the frequency domain,” *Journal of the Acoustical Society of America*, vol. 103, pp. 49–63, 1998. DOI: 10.1121/1.421106.

[5] M. Berggren, A. Bernland, and D. Noreland, “Acoustic boundary layers as boundary conditions,” *Journal of Computational Physics*, vol. 371, pp. 633–650, 2018. DOI: 10.1016/j.jcp.2018.06.005.

[6] M. P. Verge et al., “Jet formation and jet velocity fluctuations in a flue organ pipe,” *Journal of the Acoustical Society of America*, vol. 95, no. 2, pp. 1119–1132, 1994. DOI: 10.1121/1.408460.

[7] A. Ernoult and B. Fabre, “Window impedance of recorder-like instruments,” *Acustica-Acta Acustica*, vol. 103, pp. 106–116, 2017. DOI: 10.3813/AAA.919037.

[8] P. Rucz, J. Angster, and A. Miklós, “Finite element simulation of radiation impedances with applications for musical instrument design,” in *ISMA2019 International Symposium on Music Acoustics*, Detmold, Germany, 2019, pp. 275–282.

[9] P. T. Nagy, P. Rucz, and A. Szabó, “Examination of jet growth and jet-drive in the recorder by means of linearized numerical and lumped models,” *Journal of Sound and Vibration*, vol. 527, p. 116 857, 2022. DOI: 10.1016/j.jsv.2022.116857.

[10] C. Bastien, A. Ernoult, and C. Fritz, “Modeling the intonation profile of a recorder,” *Proceedings of Meetings on Acoustics*, vol. 58, no. 1, p. 035 021, 2025. DOI: 10.1121/2.0002181.

[11] S. Adachi, “Resonance modes of a flute with one open tone hole,” *Acoustical Science and Technology*, vol. 38, no. 1, pp. 14–22, 2017. DOI: 10.1250/ast.38.14.